

Record Enhancement of Curie Temperature in Host–Guest Inclusion Ferroelectrics

Xian-Jiang Song, Tie Zhang, Zhu-Xiao Gu, Zhi-Xu Zhang, Da-Wei Fu,* Xiao-Gang Chen, Han-Yue Zhang, and Ren-Gen Xiong*



Cite This: *J. Am. Chem. Soc.* 2021, 143, 5091–5098



Read Online

ACCESS |

Metrics & More

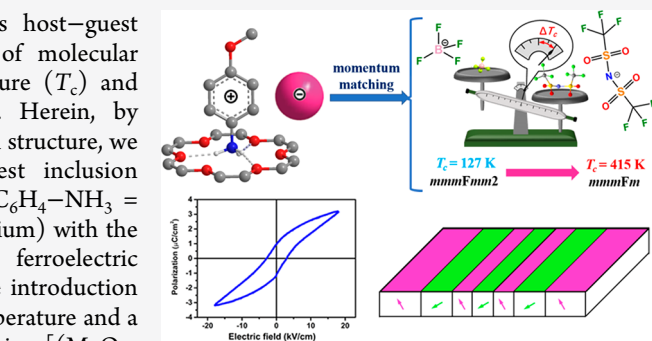
Article Recommendations

Supporting Information

ABSTRACT: Solid-state molecular rotor-type materials such as host–guest inclusion compounds are very desirable for the construction of molecular ferroelectrics. However, they usually have a low Curie temperature (T_c) and uniaxial nature, severely hindering their practical applications. Herein, by regulating the anion to control “momentum matching” in the crystal structure, we successfully designed a high-temperature multiaxial host–guest inclusion ferroelectric $[(\text{MeO}-\text{C}_6\text{H}_4-\text{NH}_3)(18\text{-crown-6})][\text{TFSA}]$ ($\text{MeO}-\text{C}_6\text{H}_4-\text{NH}_3 = 4\text{-methoxyanilinium}$, TFSA = bis(trifluoromethanesulfonyl)ammonium) with the Aizu notation of $mmmFm$. Compared to the parent uniaxial ferroelectric $[(\text{MeO}-\text{C}_6\text{H}_4-\text{NH}_3)(18\text{-crown-6})][\text{BF}_4]$ with a T_c of 127 K, the introduction of larger TFSA anions brings a lower crystal symmetry at room temperature and a higher energy barrier of molecular motions in phase transition, giving $[(\text{MeO}-\text{C}_6\text{H}_4-\text{NH}_3)(18\text{-crown-6})][\text{TFSA}]$ multiaxial ferroelectricity and a high T_c up to 415 K (above that of BaTiO_3). To our knowledge, such a record temperature enhancement of 288 K makes its T_c the highest among the reported crown-ether-based ferroelectrics, giving a wide working temperature range for applications in data storage, temperature sensing, actuation, and so on. This work will provide guidance and inspiration for designing high- T_c host–guest inclusion ferroelectrics.

INTRODUCTION

Great interest has been captured in molecular ferroelectrics as viable alternatives to conventional inorganic ferroelectrics, by taking advantage of their lightweight, low acoustic impedance, and mechanical flexibility.¹ In the past decade, remarkable progress in molecular ferroelectrics has been witnessed with the breakthrough of superior performance catching up with inorganic perovskites, making them a competitive candidate for next-generation flexible and wearable electronic devices in temperature sensing, data storage, mechanical actuation, etc.² Toward molecular ferroelectrics, the phase transition and ferroelectric mechanism are generally closely related to molecular motion and the ordered alignment of dipole moments.³ On the basis of this, the host–guest inclusion compounds represented by crown-ether-based compounds are very promising candidates for molecular ferroelectrics, because some rotational/swing motion or local twisting motion can be easily triggered in some so-called molecular machines, thereby to induce an order–disorder-type phase transition.⁴ Generally, the crown-ether molecule acts as a host to anchor a guest cation by N–H…O hydrogen-bonding interactions and assembles with the counterpart anion to form a molecular rotor-type system.⁵ By using this structural mode, several molecular ferroelectrics,⁶ such as $[(\text{MeO}-\text{C}_6\text{H}_4-\text{NH}_3)(18\text{-crown-6})][\text{BF}_4]$ ($\text{MeO}-\text{C}_6\text{H}_4-\text{NH}_3 = 4\text{-methoxyanilinium}$),⁷



$[(\text{MeO}-\text{C}_6\text{H}_4-\text{NH}_3)(18\text{-crown-6})][\text{ReO}_4]^{8}$ and $[(\text{DIPA})-(18\text{-crown-6})][\text{ClO}_4]$ (DIPA = 2,6-diisopropylanilinium), have been successfully synthesized. But unfortunately, up to now, an overwhelming majority of crown-ether-based host–guest compounds have a low Curie temperature (T_c) (usually far below room temperature) and uniaxial nature, severely hindering their applications. There exists some great difficulties and urgent tasks in this system: (i) developing high- T_c molecular ferroelectrics with a multiaxial nature and (ii) feasible design methods and strategies need to be explored and tried.

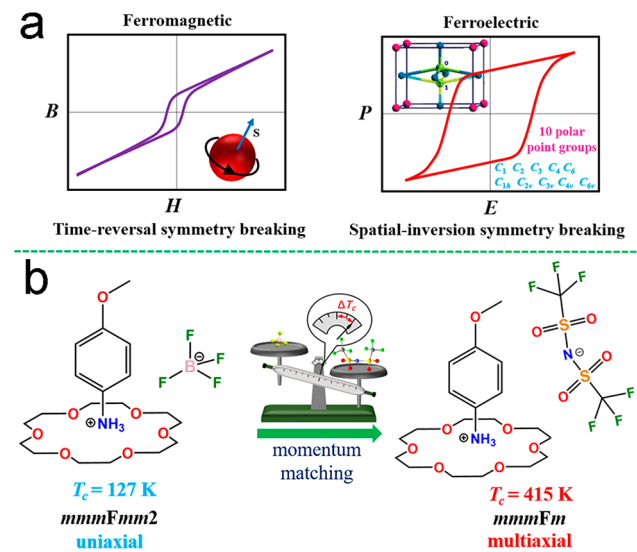
The term “ferroelectricity” is derived from ferromagnetism, while they are widely divergent (Scheme 1a). Unlike ferromagnetism, the generation of ferroelectricity is caused by the crystal structural polarity from the breaking of spatial symmetry.^{3c,10} In the molecular system, the molecular structure has a vital impact on the crystal structure, which determines that ferroelectricity can be achieved through

Received: January 18, 2021

Published: March 23, 2021



Scheme 1. (a) Comparison of Ferromagnetism and Ferroelectricity and (b) Design Concept and Strategy of High- T_c and Multiaxial Ferroelectric $[(\text{MeO}-\text{C}_6\text{H}_4-\text{NH}_3)(18\text{-crown-6})][\text{TFSA}]$



rational molecular design.¹¹ Molecular crystals are formed by connecting the internal components through weak interactions, which play an essential role in both the crystal structure and physical properties.¹² It means that there needs to be a delicate balance between cations and anions to induce and control the ferroelectricity, which is described as “momentum matching” by Zhang et al.¹³ Specifically, the size and weight of the components affect the steric hindrance and energy barrier, and meanwhile, the intermolecular interactions act like a rope pulling on each molecule in the

crystal, both of which contribute to affect the molecular motion and crystal symmetry to reasonably induce and regulate ferroelectric properties. In this stage, can the momentum matching also apply to crown-ether-based host–guest compounds to realize the high T_c and multiaxial nature?

In this work, on the basis of the reported ferroelectric, $[(\text{MeO}-\text{C}_6\text{H}_4-\text{NH}_3)(18\text{-crown-6})][\text{BF}_4]$, which undergoes an order–disorder phase transition from $Pna2_1$ to $Pnma$ at 127 K, we replaced the anions with larger TFSA (TFSA = bis(trifluoromethanesulfonyl)ammonium) to construct $[(\text{MeO}-\text{C}_6\text{H}_4-\text{NH}_3)(18\text{-crown-6})][\text{TFSA}]$ (Scheme 1b). The introduction of a larger TFSA anion changes the environment inside the crystal, bringing new C–H···O–S interactions between $(\text{MeO}-\text{C}_6\text{H}_4-\text{NH}_3)^+$ cations and TFSA anions and a high-energy barrier of molecular motions, which causes a lower symmetry at room temperature and is favorable for multiaxial ferroelectricity. Excitingly, as expected, $[(\text{MeO}-\text{C}_6\text{H}_4-\text{NH}_3)(18\text{-crown-6})][\text{TFSA}]$ is a multiaxial ferroelectric with the Aizu notation of $mmmF\bar{m}m$,¹⁴ whose T_c gets successfully increased up to 415 K. Such a dramatic enhancement of 288 K compared to that of the parent compound is the largest among the reported enhancements for molecular ferroelectrics, larger than the previous record of 229 K from (1-azabicyclo[2.2.1]heptane) CdCl_3 ($T_c = 190 \text{ K}$) to (4-fluoro-1-azabicyclo[2.2.1]heptane) CdCl_3 ($T_c = 419 \text{ K}$), representing an important step toward designing high- T_c molecular ferroelectrics.^{2e} Moreover, as far as we know, the T_c of $[(\text{MeO}-\text{C}_6\text{H}_4-\text{NH}_3)(18\text{-crown-6})][\text{TFSA}]$ is the highest one among those of the reported crown-ether-based ferroelectrics. These findings provide an effective strategy for improving the ferroelectricity and should inspire further exploration of the interplay between molecular structure and ferroelectricity.

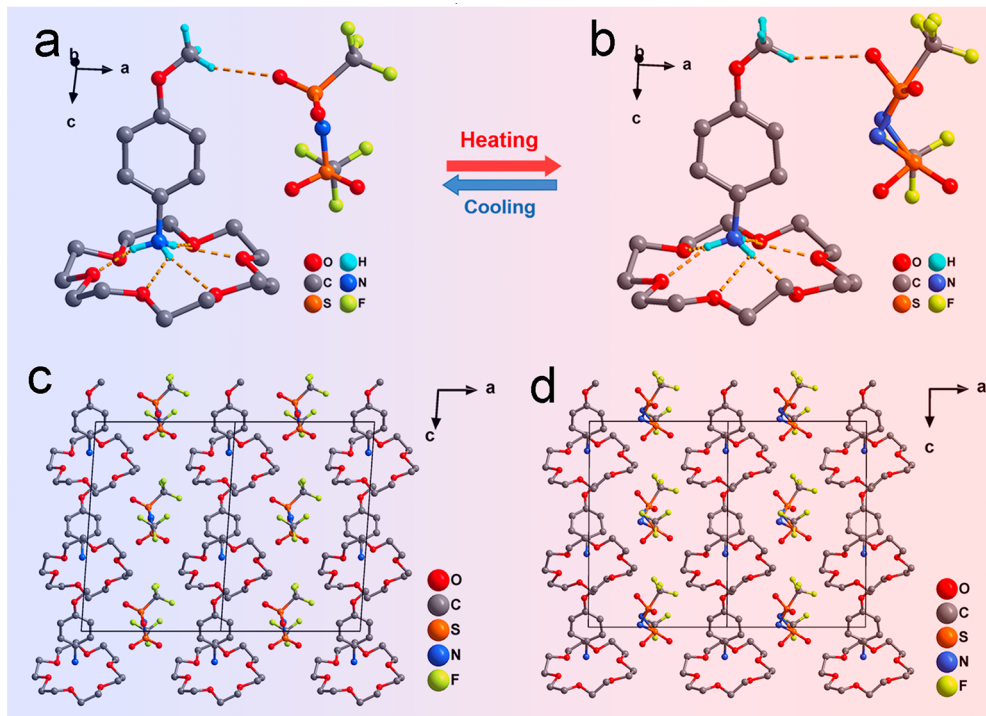


Figure 1. Crystal structures of $[(\text{MeO}-\text{C}_6\text{H}_4-\text{NH}_3)(18\text{-crown-6})][\text{TFSA}]$. The basic structures at (a) 283 K (RTP) and (b) 333 K (ITP), respectively. Packing view of structures in (c) RTP and (d) ITP, respectively. Parts of hydrogen atoms were omitted for clarity.

■ RESULTS AND DISCUSSION

The crystals of $[(\text{MeO}-\text{C}_6\text{H}_4-\text{NH}_3)(18\text{-crown-6})][\text{TFSA}]$ were easily prepared by the slow evaporation of a methanol solution of 4-methoxyaniline, 18-crown-6, and bis-(trifluoromethanesulfonyl)amine in an equimolar ratio. At 283 K (in room-temperature phase, RTP), $[(\text{MeO}-\text{C}_6\text{H}_4-\text{NH}_3)(18\text{-crown-6})][\text{TFSA}]$ crystallizes in monoclinic space group P_c , belonging to the polar point group m , with cell parameters of $a = 11.092(2)$ Å, $b = 8.4140(13)$ Å, $c = 16.627(3)$ Å, and $\beta = 93.965(15)^\circ$ (Table S1). The basic unit is composed of one host 18-crown-6 molecule and one guest $(\text{MeO}-\text{C}_6\text{H}_4-\text{NH}_3)^+$ cation with one TFSA existing as a counterpart anion. The protonated $(\text{MeO}-\text{C}_6\text{H}_4-\text{NH}_3)^+$ cation is situated in the cavity of the 18-crown-6 molecule via N–H…O hydrogen-bonding interactions to form a supramolecular complex cation, which is loosely connected to the TFSA anion through weak interactions (Figure 1a).

Compared to $[(\text{MeO}-\text{C}_6\text{H}_4-\text{NH}_3)(18\text{-crown-6})][\text{BF}_4]$, notably, new obvious C–H…O–S interactions between $(\text{MeO}-\text{C}_6\text{H}_4-\text{NH}_3)^+$ cations and the relatively large TFSA anions can be observed in $[(\text{MeO}-\text{C}_6\text{H}_4-\text{NH}_3)(18\text{-crown-6})][\text{TFSA}]$ (Figure S1), which pull each other like a rope between cations and anions. Combined with the steric hindrance from the size of TFSA anions, these attributes make $[(\text{MeO}-\text{C}_6\text{H}_4-\text{NH}_3)(18\text{-crown-6})][\text{TFSA}]$ adopt a polar crystal structure at room temperature, which was modeled as an ordered state. From the packing view, the supramolecular complex cations are arranged in two manners while the TFSA anions are located in the interstitial voids (Figure S2a), by the symmetry operation of glide planes perpendicular to the [010] direction.

Differential scanning calorimetry (DSC) analysis revealed that $[(\text{MeO}-\text{C}_6\text{H}_4-\text{NH}_3)(18\text{-crown-6})][\text{TFSA}]$ experiences three phase transitions at around $T_1 = 264$ K, $T_2 = 311$ K, and $T_3 = 415$ K (T_c), respectively (Figure 2a and Figure S3). We thus further determined its crystal structure at 333 K in the intermediate-temperate phase (ITP) and 93 K in the low-temperate phase (LTP), respectively. In ITP, $[(\text{MeO}-\text{C}_6\text{H}_4-\text{NH}_3)(18\text{-crown-6})][\text{TFSA}]$ still crystallizes in the monoclinic polar space group P_c , with cell parameters of $a = 11.229(2)$ Å, $b = 8.440(2)$ Å, $c = 16.649(4)$ Å, and $\beta = 90.30^\circ$ (Table S1). The packing view of the structure is similar to that in RTP (Figure S2). It is noteworthy that the C–H…O–S interactions between $(\text{MeO}-\text{C}_6\text{H}_4-\text{NH}_3)^+$ cations and TFSA anions also become weaker with the distance changing from 3.266 to 3.445 Å (Table S2). The N–H…O hydrogen-bond distances become weaker from RTP to ITP as well. In LTP, $[(\text{MeO}-\text{C}_6\text{H}_4-\text{NH}_3)(18\text{-crown-6})][\text{TFSA}]$ shows a freezingly ordered state, as detailed in the Supporting Information (Figure S4). From LTP to HTP, the thermal ellipsoids of all atoms become larger and bigger, especially for some F and N atoms (Figure S5), which means that the thermal vibrations of atoms become more intense. In ITP, despite occupying general symmetry positions, TFSA anions show a certain degree of disorder, and thus, the atomic coordinates of the F atom and N atom in the TFSA anion needed to be split over two positions for a better structural refinement result (Figure 1b). Therefore, the phase transition mechanism of $[(\text{MeO}-\text{C}_6\text{H}_4-\text{NH}_3)(18\text{-crown-6})][\text{TFSA}]$ can be attributed to a molecular order-disorder transition. In ITP, the TFSA anions exhibit some swing or local twisting motion, while the 18-crown-6 molecules and $(\text{MeO}-\text{C}_6\text{H}_4-\text{NH}_3)^+$ cations can be refined as an ordered model.

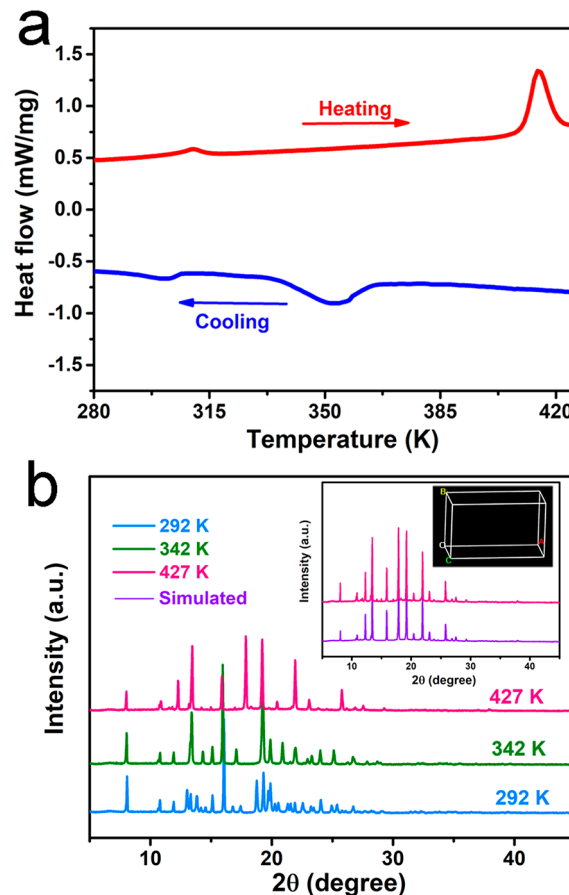


Figure 2. Phase transition behaviors of $[(\text{MeO}-\text{C}_6\text{H}_4-\text{NH}_3)(18\text{-crown-6})][\text{TFSA}]$. (a) DSC curves in the heating–cooling cycle. (b) Variable-temperature PXRD patterns; Inset: Pawley refinement of PXRD data collected at 427 K with an orthorhombic unit cell.

Structurally, in both RTP and ITP (ferroelectric phases), a striking feature is that all the C–O bonds of $(\text{MeO}-\text{C}_6\text{H}_4-\text{NH}_3)^+$ cations arrange along the same direction (Figure 1c,d), which should result in crystal polarity to induce the spontaneous polarization.

The crystal structure of $[(\text{MeO}-\text{C}_6\text{H}_4-\text{NH}_3)(18\text{-crown-6})][\text{TFSA}]$ in the high-temperature phase (HTP) was not successfully determined after many attempts, owing to the poor single-crystal X-ray diffraction data in HTP. We then performed variable-temperature powder X-ray diffraction (PXRD) measurements to explore the structural phase transitions. The PXRD patterns obtained at 292 and 342 K match well with the results simulated from the single-crystal structure (Figure S6), unraveling the high crystallinity and phase purity. The obvious difference between PXRD patterns at 292 and 342 K confirms the phase transition from RTP to ITP (Figure 2b and Figure S7). With the temperature increasing above 415 K, the pattern shows some changes again in the number and positions of diffraction peaks, meaning the emergence of a new phase (HTP). We carried out the Pawley refinements on PXRD data in HTP to get insight on some structural information (Figure S8 and inset of Figure 2b). The refined results revealed an orthorhombic cell with the point group mmm , among which the obtained most possible space group was determined as P_{cc} (see the Supporting Information for detailed refinement results).

The crystal symmetry breaking of paraelectric–ferroelectric phase transition for $[(\text{MeO}-\text{C}_6\text{H}_4-\text{NH}_3)(18\text{-crown-6})][\text{TFSA}]$ also can be investigated by second harmonic generation (SHG) experiments, because SHG response only exists in non-centrosymmetric point groups (except one of 422, 432, and 622). As shown in Figure 3a, at room

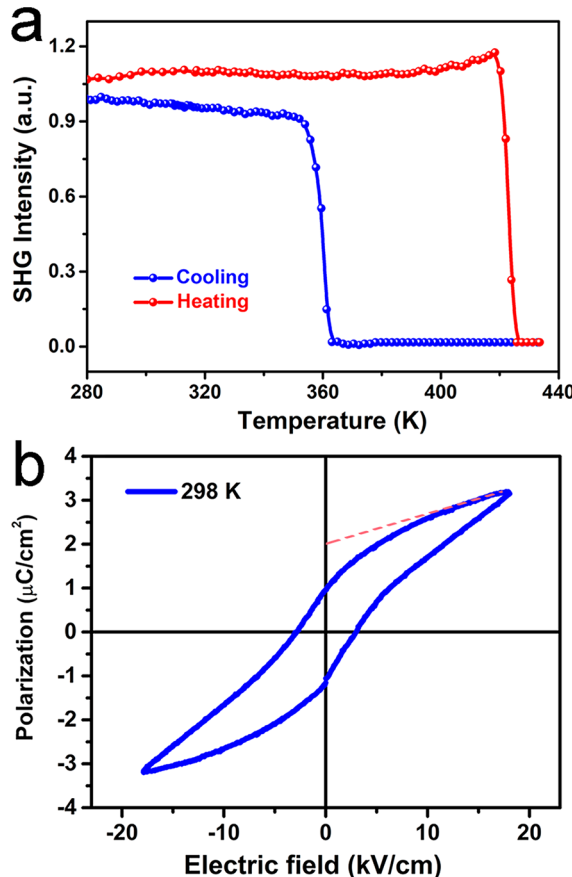


Figure 3. SHG response and ferroelectricity of $[(\text{MeO}-\text{C}_6\text{H}_4-\text{NH}_3)(18\text{-crown-6})][\text{TFSA}]$. (a) Temperature-dependent SHG response. (b) Polarization–electric field (P – E) hysteresis loop measured at 298 K.

temperature, $[(\text{MeO}-\text{C}_6\text{H}_4-\text{NH}_3)(18\text{-crown-6})][\text{TFSA}]$ shows a clear SHG response, in accordance with the polar P_c space group. No obvious SHG change was observed during the phase transition at T_2 and the SHG response remained active, due to the isostructural nature in RTP and ITP. With the temperature increased up to T_3 , the SHG intensity suddenly dropped to zero and then kept a non-active state in HTP, consistent with the centrosymmetric mmm point group from the refined results.

The paraelectric–ferroelectric phase transition of $[(\text{MeO}-\text{C}_6\text{H}_4-\text{NH}_3)][\text{TFSA}]$ belongs to $mmmFm$ type, which means that it is a multiaxial ferroelectric with two polar axes. To be the best of our knowledge, the Curie temperature (T_c , 415 K) of $[(\text{MeO}-\text{C}_6\text{H}_4-\text{NH}_3)(18\text{-crown-6})][\text{TFSA}]$ is the highest one among the reported crown-ether-based host–guest ferroelectrics, even above that (393 K) of inorganic ferroelectric BaTiO_3 .¹⁵ More strikingly, compared to the parent $[(\text{MeO}-\text{C}_6\text{H}_4-\text{NH}_3)(18\text{-crown-6})][\text{BF}_4]$, the dramatic enhancement of 288 K for T_c is the largest among reported enhancements for molecular ferroelectrics, giving $[(\text{MeO}-$

$\text{C}_6\text{H}_4-\text{NH}_3)(18\text{-crown-6})][\text{TFSA}]$ a wide working temperature range.^{2e} The ferroelectricity of $[(\text{MeO}-\text{C}_6\text{H}_4-\text{NH}_3)(18\text{-crown-6})][\text{TFSA}]$ was directly verified by the typical polarization–electric field (P – E) hysteresis loop measured on a thin film at 298 K (Figure 3b). The measured spontaneous polarization (P_s) was around $2 \mu\text{C}/\text{cm}^2$ with a remanent polarization (P_r) of $1.02 \mu\text{C}/\text{cm}^2$, and the corresponding coercive field (E_c) was about $3 \text{kV}/\text{cm}$. Such a value of P_s is larger than that of the first molecular ferroelectric Rochelle salt ($0.25 \mu\text{C}/\text{cm}^2$)¹⁰ and those of most crown-ether-based ferroelectrics including parent $[(\text{MeO}-\text{C}_6\text{H}_4-\text{NH}_3)(18\text{-crown-6})][\text{BF}_4]$ ($0.54 \mu\text{C}/\text{cm}^2$),⁷ $[(\text{MeO}-\text{C}_6\text{H}_4-\text{NH}_3)(18\text{-crown-6})][\text{ReO}_4]$ ($1.2 \mu\text{C}/\text{cm}^2$),⁸ $[(\text{DIPA})(18\text{-crown-6})][\text{BF}_4]$ ($0.3 \mu\text{C}/\text{cm}^2$),^{6b} $\text{Ca}(\text{NO}_3)_2(15\text{-crown-5})$ ($0.5 \mu\text{C}/\text{cm}^2$),^{6c} and $[(\text{DIPA})(18\text{-crown-6})][\text{ClO}_4]$ ($0.35 \mu\text{C}/\text{cm}^2$).⁹

For the momentum matching, the momentum here involves various molecular motions, such as swing motion or local twisting motion that was observed in $[(\text{MeO}-\text{C}_6\text{H}_4-\text{NH}_3)(18\text{-crown-6})][\text{BF}_4]$ and $[(\text{MeO}-\text{C}_6\text{H}_4-\text{NH}_3)(18\text{-crown-6})][\text{TFSA}]$, rotational motion, translational motion, and vibrational motion. The momentum of these motions mainly depends on the size and weight of molecules, especially the intermolecular interaction between the components, just like the rope connecting and pulling them. To further clarify the effect of intermolecular interactions on the crystal structure and properties, both Hirshfeld surfaces and two-dimensional (2D) fingerprint plots were calculated and analyzed (Figure 4).

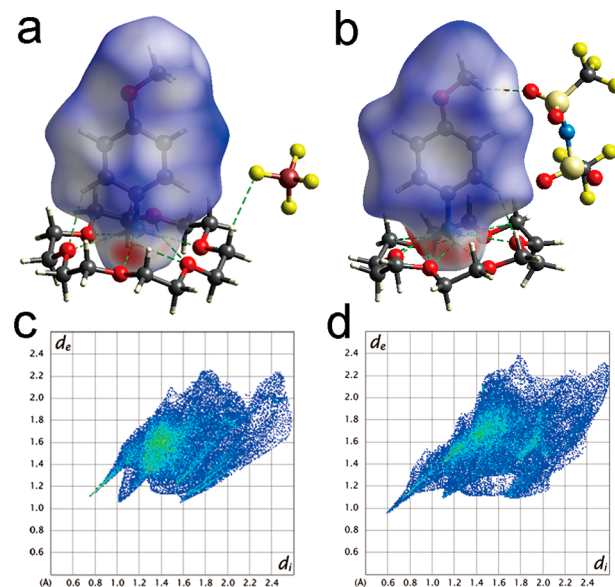


Figure 4. Comparison for Hirshfeld d_{norm} surfaces of $(\text{MeO}-\text{C}_6\text{H}_4-\text{NH}_3)^+$ cations in (a) $[(\text{MeO}-\text{C}_6\text{H}_4-\text{NH}_3)(18\text{-crown-6})][\text{BF}_4]$ and (b) $[(\text{MeO}-\text{C}_6\text{H}_4-\text{NH}_3)(18\text{-crown-6})][\text{TFSA}]$. Comparison for 2D fingerprint plots of $(\text{MeO}-\text{C}_6\text{H}_4-\text{NH}_3)^+$ cations in (c) $[(\text{MeO}-\text{C}_6\text{H}_4-\text{NH}_3)(18\text{-crown-6})][\text{BF}_4]$ and (d) $[(\text{MeO}-\text{C}_6\text{H}_4-\text{NH}_3)(18\text{-crown-6})][\text{TFSA}]$.

From the Hirshfeld surfaces, obviously, the interactions between the $(\text{MeO}-\text{C}_6\text{H}_4-\text{NH}_3)^+$ cation and surrounding molecules in $[(\text{MeO}-\text{C}_6\text{H}_4-\text{NH}_3)(18\text{-crown-6})][\text{TFSA}]$ are stronger than those in $[(\text{MeO}-\text{C}_6\text{H}_4-\text{NH}_3)(18\text{-crown-6})][\text{BF}_4]$, which can also be directly seen from the minimum (d_i , d_e) in the 2D fingerprint plots of $[(\text{MeO}-\text{C}_6\text{H}_4-\text{NH}_3)(18\text{-crown-6})][\text{TFSA}]$ (0.594, 0.956) and those of $[(\text{MeO}-\text{C}_6\text{H}_4-\text{NH}_3)(18\text{-crown-6})][\text{BF}_4]$ (0.756, 1.000). Notably,

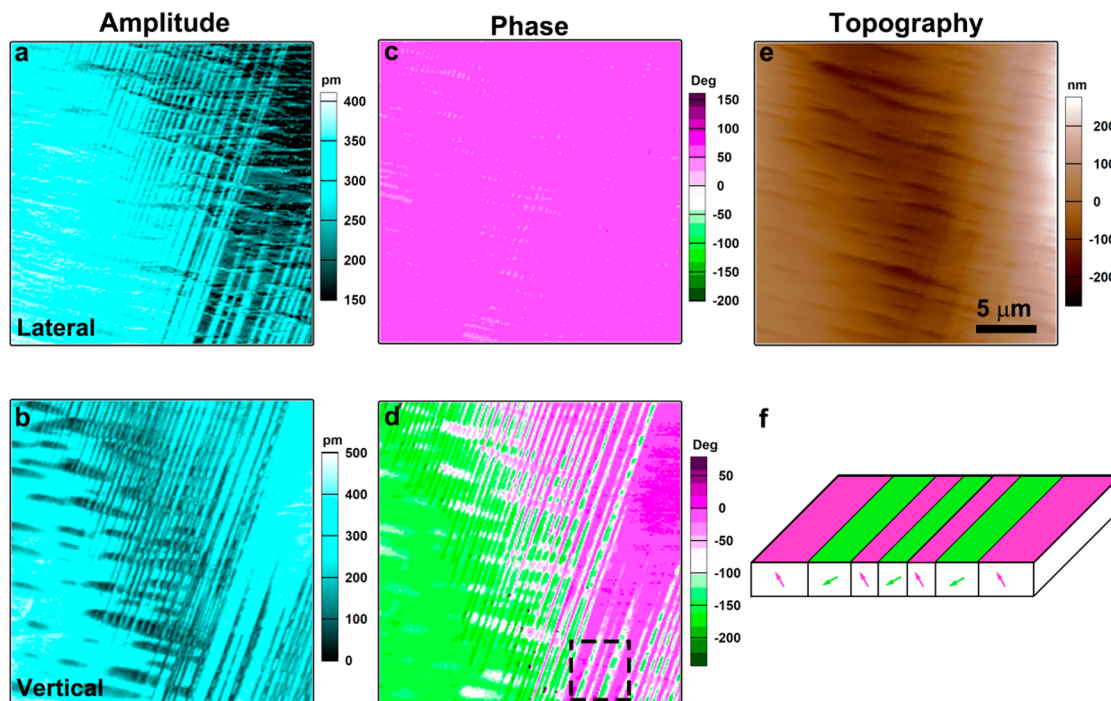


Figure 5. Micrographs from PFM including (a) lateral amplitude, (b) vertical amplitude, (c) lateral phase, (d) vertical phase, and (e) topography taken on the same region in a thin film of $[(\text{MeO}-\text{C}_6\text{H}_4-\text{NH}_3)(18\text{-crown-6})][\text{TFSA}]$. (f) Two orientations of the polarization (indicated by the arrows) in the domains around the box region in panel d.

compared to $[(\text{MeO}-\text{C}_6\text{H}_4-\text{NH}_3)(18\text{-crown-6})]\text{[BF}_4]$, new contacts (especially C–H \cdots O–S interactions) between $(\text{MeO}-\text{C}_6\text{H}_4-\text{NH}_3)^+$ cations and TFSA anions have emerged in $[(\text{MeO}-\text{C}_6\text{H}_4-\text{NH}_3)(18\text{-crown-6})]\text{[TFSA]}$, which plays a significant role in the freezing and ordering alignment of $(\text{MeO}-\text{C}_6\text{H}_4-\text{NH}_3)^+$ cations, leading to high-temperature ferroelectricity.

From Figure S9, we also observed that the interactions surrounding both anions and 18-crown-6 molecules in $[(\text{MeO}-\text{C}_6\text{H}_4-\text{NH}_3)(18\text{-crown-6})]\text{[TFSA]}$ are stronger than those in $[(\text{MeO}-\text{C}_6\text{H}_4-\text{NH}_3)(18\text{-crown-6})]\text{[BF}_4]$. In combination with the larger weight and size of TFSA anions, the strengthening of interactions could increase potential energy barrier of molecular motion and make the dipole components become ordered, resulting in a high T_c of 415 K and a lower crystal symmetry at ferroelectric phase that facilitates multiaxial ferroelectricity.

We further probed the ferroelectric nature of $[(\text{MeO}-\text{C}_6\text{H}_4-\text{NH}_3)(18\text{-crown-6})]\text{[TFSA]}$ in its thin film sample by using piezoresponse force microscopy (PFM). Briefly, PFM scans the sample surface with a conductive tip to apply a voltage and maps the local piezoresponse to this voltage, tracking local lattice deformation in both vertical and lateral modes. The information on local lattice deformation was recorded as amplitude and phase parameters, representing the piezoresponse intensity and polarization orientation, respectively. Figure 5 shows the PFM images in a thin film of $[(\text{MeO}-\text{C}_6\text{H}_4-\text{NH}_3)(18\text{-crown-6})]\text{[TFSA]}$ prepared by a drop-casting method at 293 K. The scanned region is a single crystal, in which the domain structure was determined by the crystal symmetry. For lateral PFM (Figure 5a,c), a stripe domain pattern can be seen in the amplitude image, corresponding to the uniform phase contrast. Thus, the in-plane polarization components of the adjacent domains are pointing the same direction. For vertical PFM (Figure 5b,d), a

stripe domain pattern can be observed in both amplitude and phase images, revealing the out-of-plane polarization components of adjacent domains pointing up or down. In terms of the amplitude images, one can see that the domain has a stronger (weaker) vertical piezoresponse corresponding to a weaker (stronger) lateral piezoresponse, indicating that the out-of-plane (in-plane) polarization component is larger. Thus, by collecting the amplitude and phase from the lateral and vertical PFM modes, the number of the polarization states of domains can be determined. An example for the domains around the box region marked in Figure 5d is shown in Figure 5f. We have observed two polarization directions with non- 180° in this region. However, since vertical PFM and lateral PFM depend on different cantilever distortion, their absolute amplitudes are not comparable. Therefore, we cannot determine the accurate polarization directions of domains. Considering the existence of 180° reversal of the existing two polarizations, it should have four polarization directions in $[(\text{MeO}-\text{C}_6\text{H}_4-\text{NH}_3)(18\text{-crown-6})]\text{[TFSA]}$, corresponding well with the *mmmFm* phase transition. Meanwhile, the domain structure in a thin film fabricated by the spin-coating method was investigated as well (Figure S10). It shows an irregular shape in the polycrystalline films. Note that the domain structures detected at 293 and 328 K were almost unchanged. This finding confirms that the crystal structures of RTP and ITP belong to same polar point group *m*, consistent with the crystal structural analysis.

The dielectrics are considered to be ferroelectrics only if their polarity can be switched by applying the voltage bias. Thus, we checked the polarization switching behavior of $[(\text{MeO}-\text{C}_6\text{H}_4-\text{NH}_3)(18\text{-crown-6})]\text{[TFSA]}$ by PFM. A scanned region with a single domain in its thin film was set as initial state (Figure 6a,b). Then, a tip bias of 50 V for a 0.5 s writing time was applied on the position marked as the sign of \times . From Figure 6c,d, successful switching was defined as a

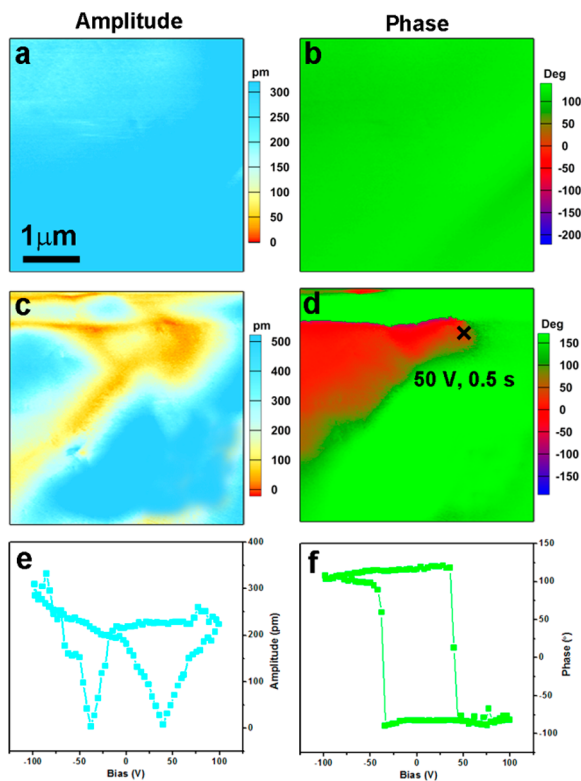


Figure 6. Polarization switching measurements for the thin film of $[(\text{MeO}-\text{C}_6\text{H}_4-\text{NH}_3)(18\text{-crown-6})][\text{TFSA}]$. (a and b) Initial PFM imaging and (c and d) after applying a 50 V voltage pulse with a 0.5 s duration on the position marked by \times in $5 \mu\text{m} \times 5 \mu\text{m}$. (e and f) PFM amplitude (e) and phase (f) signals as a function of dc tip bias.

180° PFM phase contrast between the two polarization states in the phase image and the presence of a well-defined domain wall in the amplitude image. The switching spectroscopy PFM (SS-PFM) measurements recorded the piezoresponse as a function of dc voltage bias.¹⁶ For ferroelectrics, the SS-PFM should yield characteristic PFM phase–voltage and amplitude–voltage loops that resemble the hysteresis loop and the strain butterfly loop, respectively, as shown in Figure 6e,f.¹⁷ The phase loop exhibits an approximate 180° shift under the reversal of the voltage bias, the characteristic ferroelectric nature of $[(\text{MeO}-\text{C}_6\text{H}_4-\text{NH}_3)(18\text{-crown-6})][\text{TFSA}]$. The amplitude loop is the strain change under an external field. In conjunction with the phase loop observed, the butterfly-type amplitude loop suggests that the strain is induced by the switching behavior of the polarization. Our PFM measurements provide solid evidence to support the existence of ferroelectricity in $[(\text{MeO}-\text{C}_6\text{H}_4-\text{NH}_3)(18\text{-crown-6})][\text{TFSA}]$.

CONCLUSION

In summary, we have successfully realized high-temperature multiaxial ferroelectricity in a host–guest inclusion compound $[(\text{MeO}-\text{C}_6\text{H}_4-\text{NH}_3)(18\text{-crown-6})][\text{TFSA}]$ through rational molecular design. The parent molecular rotor-type ferroelectric $[(\text{MeO}-\text{C}_6\text{H}_4-\text{NH}_3)(18\text{-crown-6})][\text{BF}_4^-]$ experiences an paraelectric–ferroelectric phase transition from $Pnma$ to $Pna2_1$ at a low T_c of 127 K. By replacing the $[\text{BF}_4^-]$ anions with larger and heavier TFSA anions, the environment inside the crystal changed and new obvious interactions between $(\text{MeO}-\text{C}_6\text{H}_4-\text{NH}_3)^+$ cations and TFSA anions were observed. These attributes decelerate the molecular dynamic

motions and make the molecules become ordered at room temperature, thereby resulting in an increased phase transition temperature and lower crystal symmetry of space group Pc for $[(\text{MeO}-\text{C}_6\text{H}_4-\text{NH}_3)(18\text{-crown-6})][\text{TFSA}]$. Just as expected, $[(\text{MeO}-\text{C}_6\text{H}_4-\text{NH}_3)(18\text{-crown-6})][\text{TFSA}]$ is a multiaxial ferroelectric with the Aizu notation of $mmmFm$, having a high T_c of 415 K, which is the highest temperature among the reported crown-ether-based host–guest inclusion ferroelectrics. Combined with the advantages of lightweight, easy processing to thin films, and environmental friendliness, $[(\text{MeO}-\text{C}_6\text{H}_4-\text{NH}_3)(18\text{-crown-6})][\text{TFSA}]$ becomes a promising and competitive candidate for sensing, actuation, data storage, flexible electronics, and biomechanical applications.

ASSOCIATED CONTENT

Supporting Information

The Supporting Information is available free of charge at <https://pubs.acs.org/doi/10.1021/jacs.1c00613>.

Discussions of experimental and characterization methods and figures of crystal structures, DSC curves, molecular structures, measured PXRD patterns, structural refinement results of PXRD data, Hirshfeld d_{norm} surfaces, domain structure detected in a thin film, ^1H , ^{13}C , and ^{19}F NMR data, and mass spectrum, and tables of crystal data and structure refinement and hydrogen bonds (PDF)

Accession Codes

CCDC 2053454–2053455 and 2064501 contain the supplementary crystallographic data for this paper. These data can be obtained free of charge via www.ccdc.cam.ac.uk/data_request/cif, or by emailing data_request@ccdc.cam.ac.uk, or by contacting The Cambridge Crystallographic Data Centre, 12 Union Road, Cambridge CB2 1EZ, UK; fax: +44 1223 336033.

AUTHOR INFORMATION

Corresponding Authors

Da-Wei Fu – Jiangsu Key Laboratory for Science and Applications of Molecular Ferroelectrics, Southeast University, Nanjing 211189, People's Republic of China; orcid.org/0000-0003-4371-097X; Email: dawei@zjnu.edu.cn

Ren-Gen Xiong – Jiangsu Key Laboratory for Science and Applications of Molecular Ferroelectrics, Southeast University, Nanjing 211189, People's Republic of China; orcid.org/0000-0003-2364-0193; Email: xiongrg@seu.edu.cn

Authors

Xian-Jiang Song – Jiangsu Key Laboratory for Science and Applications of Molecular Ferroelectrics, Southeast University, Nanjing 211189, People's Republic of China

Tie Zhang – Jiangsu Key Laboratory for Science and Applications of Molecular Ferroelectrics, Southeast University, Nanjing 211189, People's Republic of China

Zhu-Xiao Gu – Jiangsu Key Laboratory for Science and Applications of Molecular Ferroelectrics, Southeast University, Nanjing 211189, People's Republic of China; orcid.org/0000-0001-7302-540X

Zhi-Xu Zhang – Jiangsu Key Laboratory for Science and Applications of Molecular Ferroelectrics, Southeast University, Nanjing 211189, People's Republic of China

Xiao-Gang Chen – Jiangsu Key Laboratory for Science and Applications of Molecular Ferroelectrics, Southeast University, Nanjing 211189, People's Republic of China

Han-Yue Zhang — Jiangsu Key Laboratory for Science and Applications of Molecular Ferroelectrics, Southeast University, Nanjing 211189, People's Republic of China

Complete contact information is available at:
<https://pubs.acs.org/10.1021/jacs.1c00613>

Notes

The authors declare no competing financial interest.

ACKNOWLEDGMENTS

This work was financially supported by the National Natural Science Foundation of China (21991142, 21991141, and 21831004).

REFERENCES

- (1) (a) Harada, J.; Shimojo, T.; Oyamaguchi, H.; Hasegawa, H.; Takahashi, Y.; Satomi, K.; Suzuki, Y.; Kawamata, J.; Inabe, T. Directionally tunable and mechanically deformable ferroelectric crystals from rotating polar globular ionic molecules. *Nat. Chem.* **2016**, *8*, 946–952. (b) Li, P.-F.; Liao, W.-Q.; Tang, Y.-Y.; Qiao, W.; Zhao, D.; Ai, Y.; Yao, Y.-F.; Xiong, R.-G. Organic enantiomeric high- T_c ferroelectrics. *Proc. Natl. Acad. Sci. U. S. A.* **2019**, *116*, 5878–5885. (c) Tang, Y. Y.; Li, P. F.; Liao, W. Q.; Shi, P. P.; You, Y. M.; Xiong, R. G. Multiaxial Molecular Ferroelectric Thin Films Bring Light to Practical Applications. *J. Am. Chem. Soc.* **2018**, *140*, 8051–8059. (d) Xu, W.-J.; Romanyuk, K.; Martinho, J. M. G.; Zeng, Y.; Zhang, X.-W.; Ushakov, A.; Shur, V.; Zhang, W.-X.; Chen, X.-M.; Kholkin, A.; Rocha, J. Photoresponsive Organic-Inorganic Hybrid Ferroelectric Designed at the Molecular Level. *J. Am. Chem. Soc.* **2020**, *142*, 16990–16998. (e) Xu, Z.; Weng, W.; Li, Y.; Liu, X.; Yang, T.; Li, M.; Huang, X.; Luo, J.; Sun, Z. 3D-to-2D Dimensional Reduction for Exploiting a Multilayered Perovskite Ferroelectric toward Polarized-Light Detection in the Solar-Blind Ultraviolet Region. *Angew. Chem., Int. Ed.* **2020**, *59*, 21693–21697.
- (2) (a) Fu, D. W.; Cai, H. L.; Liu, Y.; Ye, Q.; Zhang, W.; Zhang, Y.; Chen, X. Y.; Giovannetti, G.; Capone, M.; Li, J.; Xiong, R. G. Diisopropylammonium bromide is a high-temperature molecular ferroelectric crystal. *Science* **2013**, *339*, 425–428. (b) Horiuchi, S.; Tokunaga, Y.; Giovannetti, G.; Picozzi, S.; Itoh, H.; Shimano, R.; Kumai, R.; Tokura, Y. Above-room-temperature ferroelectricity in a single-component molecular crystal. *Nature* **2010**, *463*, 789. (c) Liao, W.-Q.; Zhao, D.; Tang, Y.-Y.; Zhang, Y.; Li, P.-F.; Shi, P.-P.; Chen, X.-G.; You, Y.-M.; Xiong, R.-G. A molecular perovskite solid solution with piezoelectricity stronger than lead zirconate titanate. *Science* **2019**, *363*, 1206. (d) Shi, C.; Ma, J.-J.; Jiang, J.-Y.; Hua, M.-M.; Xu, Q.; Yu, H.; Zhang, Y.; Ye, H.-Y. Large Piezoelectric Response in Hybrid Rare-Earth Double Perovskite Relaxor Ferroelectrics. *J. Am. Chem. Soc.* **2020**, *142* (21), 9634–9641. (e) Tang, Y.-Y.; Xie, Y.; Zeng, Y.-L.; Liu, J.-C.; He, W.-H.; Huang, X.-Q.; Xiong, R.-G. Record Enhancement of Phase Transition Temperature Realized by H/F Substitution. *Adv. Mater.* **2020**, *32*, 2003530. (f) Ye, H.-Y.; Tang, Y.-Y.; Li, P.-F.; Liao, W.-Q.; Gao, J.-X.; Hua, X.-N.; Cai, H.; Shi, P.-P.; You, Y.-M.; Xiong, R.-G. Metal-free three-dimensional perovskite ferroelectrics. *Science* **2018**, *361*, 151. (g) You, Y.-M.; Liao, W.-Q.; Zhao, D.; Ye, H.-Y.; Zhang, Y.; Zhou, Q.; Niu, X.; Wang, J.; Li, P.-F.; Fu, D.-W.; Wang, Z.; Gao, S.; Yang, K.; Liu, J.-M.; Li, J.; Yan, Y.; Xiong, R.-G. An organic-inorganic perovskite ferroelectric with large piezoelectric response. *Science* **2017**, *357*, 306.
- (3) (a) Peng, Y.; Bie, J.; Liu, X.; Li, L.; Chen, S.; Fa, W.; Wang, S.; Sun, Z.; Luo, J. Acquiring High-TC Layered Metal Halide Ferroelectrics via Cage-Confining Ethylamine Rotators. *Angew. Chem., Int. Ed.* **2020**, *60* (6), 2839–2843. (b) Sato, O. Dynamic molecular crystals with switchable physical properties. *Nat. Chem.* **2016**, *8*, 644–656. (c) Shi, P. P.; Tang, Y. Y.; Li, P. F.; Liao, W. Q.; Wang, Z. X.; Ye, Q.; Xiong, R. G. Symmetry breaking in molecular ferroelectrics. *Chem. Soc. Rev.* **2016**, *45*, 3811–3827. (d) Tayi, A. S.; Kaeser, A.; Matsumoto, M.; Aida, T.; Stupp, S. I. Supramolecular ferroelectrics. *Nat. Chem.* **2015**, *7*, 281–294.
- (4) (a) Akutagawa, T.; Koshinaka, H.; Sato, D.; Takeda, S.; Noro, S.-I.; Takahashi, H.; Kumai, R.; Tokura, Y.; Nakamura, T. Ferroelectricity and polarity control in solid-state flip-flop supramolecular rotators. *Nat. Mater.* **2009**, *8*, 342. (b) Akutagawa, T.; Nakamura, T. Supramolecular approach for solid state Brownian rotators. *Dalton Trans.* **2008**, 6335–6345. (c) Garcia-Garibay, M. A. Crystalline molecular machines: Encoding supramolecular dynamics into molecular structure. *Proc. Natl. Acad. Sci. U. S. A.* **2005**, *102*, 10771. (d) Horansky, R. D.; Clarke, L. I.; Price, J. C.; Khuong, T. A. V.; Jarowski, P. D.; Garcia-Garibay, M. A. Dielectric response of a dipolar molecular rotor crystal. *Phys. Rev. B* **2005**, *72* (1), 014302.
- (5) (a) Akutagawa, T.; Sato, D.; Koshinaka, H.; Aonuma, M.; Noro, S.-I.; Takeda, S.; Nakamura, T. Solid-State Molecular Rotators of Anilinium and Adamantylammonium in [Ni(dmit)₂]⁻ Salts with Diverse Magnetic Properties. *Inorg. Chem.* **2008**, *47*, 5951–5962. (b) Li, W.; He, C. T.; Zeng, Y.; Ji, C. M.; Du, Z. Y.; Zhang, W. X.; Chen, X. M. Crystalline Supramolecular Gyroscope with a Water Molecule as an Ultrasmall Polar Rotator Modulated by Charge-Assisted Hydrogen Bonds. *J. Am. Chem. Soc.* **2017**, *139*, 8086–8089.
- (6) (a) Tang, Y. Z.; Yu, Y. M.; Xiong, J. B.; Tan, Y. H.; Wen, H. R. Unusual High-Temperature Reversible Phase-Transition Behavior, Structures, and Dielectric-Ferroelectric Properties of Two New Crown Ether Clathrates. *J. Am. Chem. Soc.* **2015**, *137*, 13345–13351. (b) Ye, H. Y.; Li, S. H.; Zhang, Y.; Zhou, L.; Deng, F.; Xiong, R. G. Solid state molecular dynamic investigation of an inclusion ferroelectric: [(2,6-diisopropylanilinium)([18]crown-6)]BF₄. *J. Am. Chem. Soc.* **2014**, *136*, 10033–10040. (c) Ye, H. Y.; Zhang, Y.; Fu, D. W.; Xiong, R. G. A displacive-type metal crown ether ferroelectric compound: Ca(NO₃)₂(15-crown-5). *Angew. Chem., Int. Ed.* **2014**, *53*, 6724–6729.
- (7) Fu, D. W.; Zhang, W.; Cai, H. L.; Zhang, Y.; Ge, J. Z.; Xiong, R. G.; Huang, S. D. Supramolecular bola-like ferroelectric: 4-methoxyanilinium tetrafluoroborate-18-crown-6. *J. Am. Chem. Soc.* **2011**, *133*, 12780–12786.
- (8) Fu, D. W.; Cai, H. L.; Li, S. H.; Ye, Q.; Zhou, L.; Zhang, W.; Zhang, Y.; Deng, F.; Xiong, R. G. 4-Methoxyanilinium perrhenate 18-crown-6: a new ferroelectric with order originating in swinglike motion slowing down. *Phys. Rev. Lett.* **2013**, *110*, 257601.
- (9) Zhang, Y.; Ye, H. Y.; Fu, D. W.; Xiong, R. G. An order-disorder ferroelectric host-guest inclusion compound. *Angew. Chem., Int. Ed.* **2014**, *53*, 2114–2118.
- (10) Zhang, W.; Xiong, R.-G. Ferroelectric Metal-Organic Frameworks. *Chem. Rev.* **2012**, *112*, 1163–1195.
- (11) Liu, H.-Y.; Zhang, H.-Y.; Chen, X.-G.; Xiong, R.-G. Molecular Design Principles for Ferroelectrics: Ferroelectrochemistry. *J. Am. Chem. Soc.* **2020**, *142*, 15205–15218.
- (12) (a) Desiraju, G. R. Crystal engineering: from molecule to crystal. *J. Am. Chem. Soc.* **2013**, *135*, 9952–9967. (b) Liao, W. Q.; Tang, Y. Y.; Li, P. F.; You, Y. M.; Xiong, R. G. Competitive Halogen Bond in the Molecular Ferroelectric with Large Piezoelectric Response. *J. Am. Chem. Soc.* **2018**, *140*, 3975–3980.
- (13) (a) Hua, X.-N.; Liao, W.-Q.; Tang, Y.-Y.; Li, P.-F.; Shi, P.-P.; Zhao, D.; Xiong, R.-G. A Room-Temperature Hybrid Lead Iodide Perovskite Ferroelectric. *J. Am. Chem. Soc.* **2018**, *140*, 12296–12302. (b) Zhang, H.-Y.; Tang, Y.-Y.; Shi, P.-P.; Xiong, R.-G. Toward the Targeted Design of Molecular Ferroelectrics: Modifying Molecular Symmetries and Homochirality. *Acc. Chem. Res.* **2019**, *52*, 1928–1938.
- (14) Aizu, K. Possible Species of Ferroelastic Crystals and of Simultaneously Ferroelectric and Ferroelastic Crystals. *J. Phys. Soc. Jpn.* **1969**, *27*, 387–396.
- (15) Haertling, G. H. Ferroelectric Ceramics: History and Technology. *J. Am. Ceram. Soc.* **1999**, *82*, 797–818.
- (16) Song, X.-J.; Zhang, Z.-X.; Chen, X.-G.; Zhang, H.-Y.; Pan, Q.; Yao, J.; You, Y.-M.; Xiong, R.-G. Bistable State of Protons for Low-Voltage Memories. *J. Am. Chem. Soc.* **2020**, *142*, 9000–9006.

(17) Liu, Y.; Weiss, D. N.; Li, J. Rapid Nanoimprinting and Excellent Piezoresponse of Polymeric Ferroelectric Nanostructures. *ACS Nano* **2010**, *4*, 83–90.